

• 土木工程 •

DOI:10.12454/j.jsuese.202400871



本刊网刊

## 锈蚀钢筋与纤维增强混凝土黏结性能试验研究

刘延春<sup>1</sup>, 陈本晟<sup>1</sup>, 刘才玮<sup>1\*</sup>, 闫良泰<sup>2</sup>, 刘新宇<sup>1</sup>, 苗吉军<sup>1</sup>

(1. 青岛理工大学 土木工程学院, 山东 青岛 266520; 2. 北京工业大学 城市建设学部, 北京 100124)

**摘要:**为研究锈蚀钢筋与玄武岩-聚丙烯纤维增强混凝土(BPFRC)的黏结滑移机理,本文应用电化学加速锈蚀方法制备了48个不同锈蚀率(0、2%、5.0%和10.0%)下的棱柱体偏心拉拔试件,通过基本力学性能试验探究纤维掺入对混凝土基体影响;开展拉拔试验观察纤维增强混凝土(FRC)黏结性能变化规律,记录试件表面变化与破坏模式;采用电镜扫描对破坏后黏结界面的微观测试。试验结果表明:1)纤维的桥接有效抑制裂缝发展并分散荷载作用,FRC的劈裂抗拉强度和抗折强度分别提高了12.43%~18.65%和5.36%~9.64%;2)在黏结性能方面,锈蚀影响下混凝土约束和界面摩擦大幅降低,钢筋锈蚀率6%~7%时,普通混凝土黏结强度平均降低18.1%,BPFRC与普通混凝土割线黏结刚度分别下降43.3%和39.0%,而初始黏结刚度受锈蚀影响较小,降低了5.0%~11.8%;3)锈蚀损伤条件下FRC在黏结强度、黏结刚度、残余强度等方面表现出一定优势,不同锈蚀率下FRC的黏结强度比普通混凝土提高11.1%~27.6%,BPFRC较玄武岩纤维增强混凝土(BFRC)/聚丙烯纤维增强混凝土(PFRC)提高了5.2%~11.8%,两种纤维混合时体现出正协同效应。在试验结果基础上,本文结合锈蚀损伤系数建立不同纤维掺入的半经验半理论黏结强度预测公式与三段式黏结-滑移本构关系。研究结果可为BF-PF增强混凝土的性能评估提供数据支持。

**关键词:**纤维增强混凝土;锈蚀;力学性能;黏结-滑移;本构模型

中图分类号:TU375

文献标志码:A

文章编号:2096-3246(2025)05-0261-13

钢筋与混凝土间黏结是影响结构性能的重要因素之一<sup>[1]</sup>,实际工程中钢筋混凝土结构不可避免地会受到氯离子侵入而引起内部钢筋锈蚀,锈蚀产物堆积会导致混凝土保护层开裂并对黏结界面的造成损伤<sup>[2]</sup>。因此,对钢筋与混凝土间黏结性能开展研究十分必要。现有研究进行了考虑多因素的系统探讨,Yalciner等<sup>[3]</sup>研究了以保护层厚度等为变量的钢筋混凝土在不同锈蚀率下的黏结行为,发现高强混凝土开裂更为严重,较低的渗透性维持了锈蚀产物的膨胀压力。王朝阳等<sup>[4]</sup>研究发现,黏结强度与黏结刚度随锈蚀率提高呈现先增大后减小趋势,且锈蚀对滑移小于0.05 mm的初始刚度影响尤为显著。Li等<sup>[5]</sup>研究了钢筋类型和配箍率对锈蚀试件黏结性能的影响,结果表明未锈蚀带肋钢筋试件的黏结强度随配箍率的增加近似呈线性增加;较高的配箍率对延缓纵筋锈蚀造成的黏结应力下降有明显效果。鉴于目前对考虑纵筋、箍筋共同锈蚀后黏结性能劣化

规律和本构关系的研究不足,杨路等<sup>[6]</sup>通过电渗-恒电流-干湿循环的加速锈蚀方法,建立并验证了考虑箍筋间距、纵筋箍筋锈蚀率等参数的黏结滑移本构模型,为锈蚀影响下的黏结关系提供了更可靠的依据。

目前纤维应用愈发广泛,纤维增强混凝土(FRC)具有更好的力学性能和耐久性,适用于多种复杂环境和严苛工程。玄武岩纤维(BF)有轻质、高强、耐腐蚀的特点;聚丙烯纤维(PF)能体现出优越的抗断裂性能<sup>[7]</sup>,合理掺量对混凝土基体强度有明显改善<sup>[8]</sup>。在黏结性能上FRC表现出新的特征,锈蚀影响下的裂缝发展及黏结退化机理与普通混凝土不同。已有研究<sup>[9-12]</sup>表明:纤维掺入可有效控制混凝土开裂,改变破坏模式并提高黏结强度;1%BF掺入使抗压强度提高1.0%~10.5%且1.5%时黏结强度增幅最大<sup>[11]</sup>;PF掺入使得黏结滑移曲线下降阶段变得更平坦,提高了试件韧性<sup>[12]</sup>。但由于纤维种类和掺量不同,既有结果无法一概而论,

收稿日期:2024-10-28 修回日期:2024-12-24 网络出版日期:2024-12-26

基金项目:国家自然科学基金项目(52178487);山东省自然科学基金项目(ZR2021ME228)

作者简介:刘延春(1971—),女,高级实验师。研究方向:结构抗火。E-mail: 65230768@qq.com

\*通信作者:刘才玮,教授, E-mail: 03150053@163.com

尚需进一步研究。此外为了寻求更好的基体性能响应,不同形式的混合纤维开始取代单一纤维形式<sup>[13-14]</sup>,以期形成具有更好性能的复合材料并观察在黏结滑移方向的表现。

现有研究大多集中于锈蚀钢筋与普通混凝土,对于不同类型FRC的黏结关系对比研究还有待开展。本文针对锈蚀钢筋和玄武岩-聚丙烯纤维增强混凝土(BFRC、PFRC、BPFRC)的黏结性能进行试验,通过对36个试件进行基本力学性能测试、48个试件进行偏心拉拔试验,探究纤维种类对混凝土基体的改善情况及锈蚀影响下的黏结退化机制。

表1 纤维特征参数

Tab. 1 Fiber specifications

类型	长度 $l_i$ /mm	直径 $d_i$ /μm	密度/(g·cm <sup>-3</sup> )	抗拉强度/MPa	弹性模量/GPa	伸长率/%
PF	18	18.1	0.92	560	7.2	33.0
BF	12	13.2	2.85	1 938	78.0	2.9

表2 混凝土配合比

Tab. 2 Mixture proportion of concrete

类型	各组分含量/(kg·m <sup>-3</sup> )								
	水泥	粉煤灰	矿粉	砂	石子	水	减水剂	BF	PF
NC	380.0	85.1	114.90	600.0	1 053.4	158.6	3.3	0	0
BFRC	380.0	85.1	114.90	600.0	1 053.4	158.6	3.3	2.850	0
PFRC	380.0	85.1	114.90	600.0	1 053.4	158.6	3.3	0	0.92
BPFRC	380.0	85.1	114.90	600.0	1 053.4	158.6	3.3	1.425	0.46

注:NC为普通混凝土,BFRC为玄武岩纤维混凝土,PFRC为聚丙烯纤维混凝土,BPFRC为玄武岩-聚丙烯纤维混凝土。

试验纵向受拉钢筋选用直径18 mm的HRB500E带肋钢筋,箍筋和架立筋为直径8 mm的HRB400钢筋。棱柱体拉拔试件尺寸为150 mm×150 mm×300 mm,黏结长度为5倍钢筋直径(90 mm),此时拉拔试件的黏结界面应力分布较为均匀。试件保护层厚度为30 mm,钢筋未黏结部分用PVC(聚氯乙烯)塑料管包裹,以隔离混凝土并防止拉拔试验时因应力集中而造成局部损坏。试件构造及尺寸如图1所示,钢筋力学性能见表3。

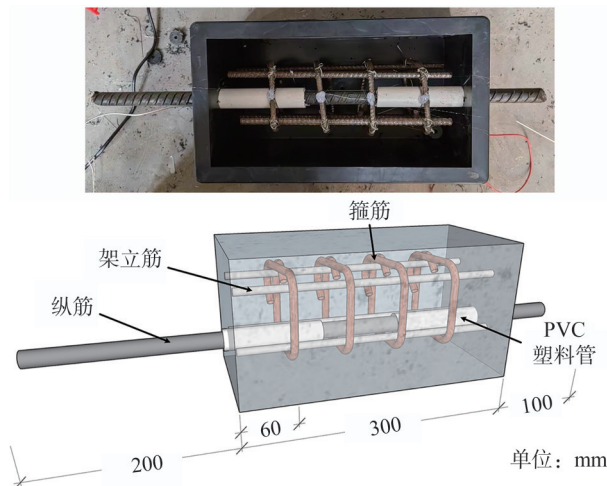


图1 试件构造及尺寸

Fig. 1 Construction and dimensions of specimen

## 1 试验概况

### 1.1 试件制备

试验混凝土设计强度为C50,水泥为42.5普通硅酸盐水泥,细骨料使用0.2~0.6 mm天然河砂,粗骨料为最大粒径25 mm的花岗岩,添加粉煤灰、矿粉和减水率25%的聚羧酸减水剂,单一纤维试件分别掺入体积分数0.1%的PF和BF(混掺纤维试件中两种纤维的体积分数各为0.05%),以期体现纤维对混凝土的改善及抵抗氯离子侵蚀的优势<sup>[15-16]</sup>,纤维特征参数如表1所示。混凝土配合比详见表2。

表3 钢筋力学性能

Tab. 3 Mechanical properties of steel bars

类型	直径 $d$ /mm	屈服强度/MPa	极限强度/MPa	弹性模量/GPa
HRB500E	18	515	657	216
HRB400	8	435	508	207

### 1.2 测试方法

#### 1.2.1 力学性能测试

制作尺寸为150 mm×150 mm×550 mm的试件进行三点弯曲试验,100 mm×100 mm×100 mm的立方体试件进行抗压和劈裂抗拉试验。所有试件同期脱模,并在标准养护条件下养护28 d。根据规范GB/T 50081—2019<sup>[17]</sup>进行试验操作,由每组3个试件得到实际强度平均值,混凝土力学试验如图2所示。

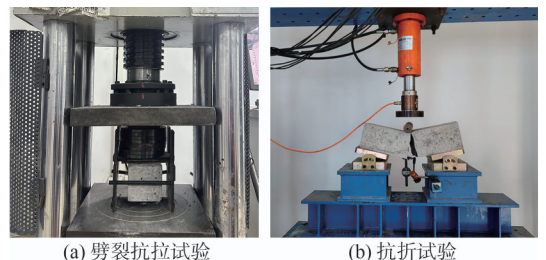


图2 混凝土力学试验

Fig. 2 Mechanical properties tests of concrete

1.2.2 加速锈蚀试验

棱柱体拉拔试件养护完毕后,采用电化学方法加速锈蚀钢筋。为模拟实际工程构件的锈蚀状态,受拉钢筋与箍筋间不进行绝缘隔氧处理。先将试件浸泡于浓度为5%的NaCl溶液中静置7 d,待溶液充分渗透到混凝土内部后再通电。将钢筋与直流电源正极相连,不锈钢棒与电源负极相连,各试件通过并联方式连接,电化学加速锈蚀示意图3所示。采用恒定电流方式,保持锈蚀电流密度为 $200 \mu\text{A}/\text{cm}^2$ 。根据法拉第定律得到通电时间与理论锈蚀率间关系,由式(1)计算。当时间达到预定值后,关闭电源并拆除钢筋上导线,将拉拔试件取出,自然晾干。

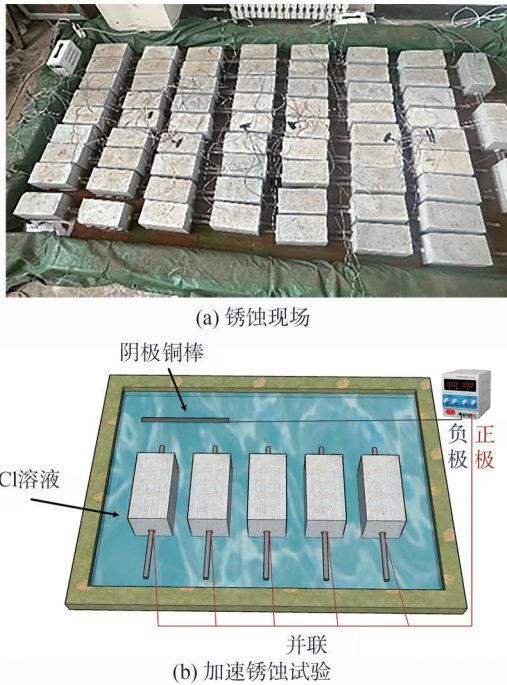


图3 电化学加速锈蚀示意图

Fig. 3 Schematic diagram of electrochemical accelerated corrosion

$$t = \frac{zFr\rho\eta_0}{2Ai} \quad (1)$$

式中, $t$ 为锈蚀持续时间, $z$ 为阳极化学价, $F$ 为法拉第常数, $r$ 为锈蚀钢筋的半径, $\rho$ 为密度, $\eta_0$ 为理论锈蚀率, $A$ 为锈蚀物的原子量, $i$ 为锈蚀电流密度。

1.2.3 拉拔测试

偏心拉拔试验在最大施荷1 000 kN的电液伺服万能试验机上进行,如图4所示。试验加载装置采用专门设计用于偏心拉拔试验的加载架,加载架由高强度钢板、约束钢板和高强度螺杆组成,以确保试件的稳定性。通过试验机的传感器测量拉拔力,并使用两个线性可变差动变压器(LVDT)测量滑移。试验采用位移加载方式,加载速率为0.5 mm/min,拉拔力下降趋于稳定或试件破坏为结束标志。

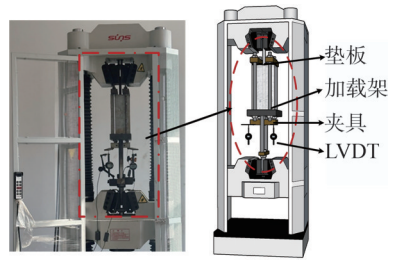


图4 拉拔测试试验装置图

Fig. 4 Pull-out test setup

黏结应力 $\tau$ 定义为钢筋与周围混凝土之间沿黏结长度的剪应力,按式(2)计算:

$$\tau = \frac{F_u}{\pi dl} \quad (2)$$

式中, $F_u$ 为试验机采集荷载, $d$ 为纵筋直径, $l$ 为黏结段长度。

1.2.4 锈蚀率测量

拉拔试验结束后使用切割机截取出黏结段钢筋,将其浸泡在质量分数为5%的盐酸中酸洗30 min,随后使用钢丝球清除钢筋表面附着混凝土及锈蚀物,然后放入防锈剂浸泡防止进一步锈蚀,最后用清水冲净并拿干毛巾擦拭,进行称重与长度测量。按质量损失法计算钢筋的实际锈蚀率 $\eta$ (式(3)),不同锈蚀率下钢筋对比如图5所示。

$$\eta = \frac{m_0 - m_c}{m_0} \times 100\% \quad (3)$$

式中, $m_0$ 为未锈蚀钢筋的单位质量, $m_c$ 为锈蚀后钢筋的单位质量。

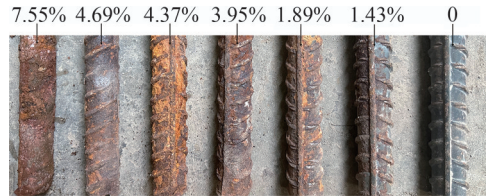


图5 不同腐蚀程度钢筋的外观

Fig. 5 Appearance diagram of steel bars with different corrosion degree

2 试验结果及分析

2.1 力学性能

力学性能试验结果如图6所示,纤维掺入提高了混凝土的抗压强度,其中,PFRC与BFRC较NC分别提高了6.49%和10.55%,纤维混掺产生了更好的效果,提升11.16%。BF较高的弹性模量在压缩变形过程中能承受更大的应力,PF弹性模量低,对混凝土抗压强度提升有限。Smarzewski<sup>[18]</sup>、赵兵兵<sup>[19]</sup>等研究发现,掺入一定量的纤维后,对混凝土强度起副作用,作为初始缺陷对密实度产生不利影响,但较均匀分布的纤维会形成3维网络结构,充分发挥桥接作用以抑制微裂缝的发展。本试验掺量下起到了利大于弊的效果。

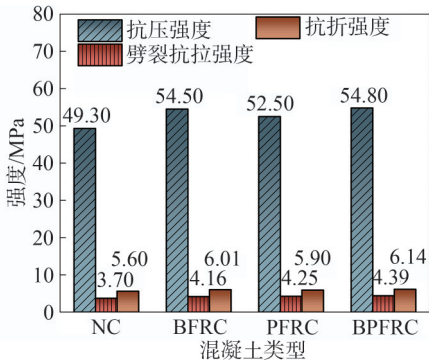


图6 力学性能测试结果

Fig. 6 Results of mechanical performance tests

单掺 PF、BF 与混掺对劈裂抗拉强度的提高幅度分别为 14.86%、12.43% 和 18.65%，归因于纤维在混凝土中如加强筋般的改善作用。BF 对微裂缝的萌生和发展具有抑制作用，PF 更侧重于限制宏观裂缝产生后的扩展延伸，两种纤维在裂缝发展不同阶段起到互补作用，体现出 PF+BF 的正协同效应。此外 NC 的抗折强度为 5.6 MPa，单掺 PF 与 BF 后强度分别提高 5.36% 和 7.32%，BPFRC 增加 9.64%。混凝土开裂时断面两侧分布的纤维提供牵拉作用，增强了其抗折强度和延性。

为定量研究纤维混掺增强效应，计算考虑弯曲度和断裂能的混掺增强效应系数  $R^{[20]}$ ，如式(4)所示：

$$R = \frac{\theta - \sum_{i=1}^n \theta_i \delta_i}{\sum_{i=1}^n \theta_i \delta_i} \quad (4)$$

式中： $\theta$ 为混杂纤维水泥基复合材料的性能指标； $\theta_i$ 为单掺  $i$  纤维的性能指标； $\delta_i$ 为单掺  $i$  纤维的体积分数， $\delta_i = V_i/V$ ， $V_i$ 为单掺  $i$  纤维的体积， $V$ 为混杂纤维的总体积， $\sum \delta_i = 1$ 。

纤维混杂效应系数如图7所示。从图7中可以看出，在混凝土中掺入 BF-PF 组合对劈裂抗拉强度的改善更为明显， $R=0.044$ 。但这与长径比、纤维分布的随机性等有着密不可分的关系，由于目前缺乏较统一的最佳混合纤维掺入比例，尚需通过试验进一步探讨变化规律。

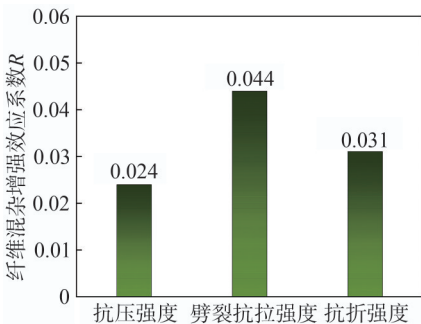


图7 纤维混杂效应系数

Fig. 7 Fiber mixing effect coefficient

## 2.2 锈蚀和破坏现象

锈蚀离散及箍筋阴极保护作用使理论锈蚀率与实际锈蚀率有一定差距，此外纤维掺入降低了混凝土的孔隙率和渗透性，纤维的表面特性影响与水分的相互作用，进而影响孔隙液中氯离子的运输。实际平均锈蚀率分别为 1.65%、4.39% 和 6.56%。如图8所示，锈蚀产物在钢筋与混凝土间堆积，随锈蚀程度的加深，混凝土表面出现锈胀裂缝且伴有红褐色锈产物溢出。

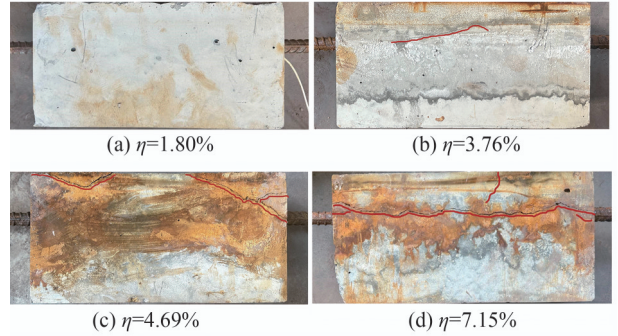


图8 锈胀裂缝

Fig. 8 Rust expansion cracks

拉拔试件均发生劈裂-拔出破坏，试件破坏模式如图9所示。试验过程中钢筋并未屈服，拉拔裂缝从加载段钢筋根部开始产生，向四周发展，其中一条主裂缝延伸至混凝土侧面，随荷载增加在侧面发展为近似平行钢筋的纵向贯穿裂缝，最终拉拔力稳定，混凝土试件发生延性破坏。钢筋笼对混凝土的横向约束以及纤维的桥接作用可有效抵抗钢筋锈蚀产生的环向锈胀力，限制裂缝发展并分散荷载作用。FRC 试件裂缝更加细微且数量较少。

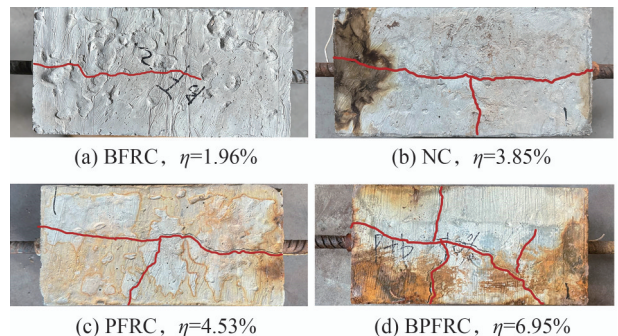


图9 试件破坏模式

Fig. 9 Specimen failure modes

## 2.3 黏结关系

拉拔试验测试数据记录于表4，不同工况下试件黏结滑移曲线如图10所示。

黏结滑移曲线可大致分为3个阶段：滑移(上升)阶段、下降阶段和残余阶段。在滑移阶段，滑移量与黏结应力近似呈线性关系，黏结应力随滑移量的增长大幅上升。由于钢筋与混凝土间化学胶结力的不断损失，在近峰值时曲线呈现出非线性特征。随着混凝土

表 4 拉拔试验结果  
Tab. 4 Results of pull-out test

试件编号	$\tau_u$ /MPa	$s_u$ /mm	$\eta$ /%	$K_i$ /(MPa·mm <sup>-1</sup> )	$K_s$ (MPa·mm <sup>-1</sup> )	试件编号	$\tau_u$ /MPa	$s_u$ /mm	$\eta$ /%	$K_i$ (MPa·mm <sup>-1</sup> )	$K_s$ (MPa·mm <sup>-1</sup> )
NC-0-1	20.12	1.15	0	43.96	21.04	NC-5-1	18.11	1.48	4.93	39.20	17.92
NC-0-2	19.28	1.38	0	45.21	19.75	NC-5-2	19.45	1.39	3.85	40.89	19.02
NC-0-3	21.08	1.46	0	46.43	22.2	NC-5-3	17.94	1.72	4.57	42.91	18.56
PFRC-0-1	22.92	1.25	0	43.61	23.43	PFRC-5-1	20.36	1.56	4.37	42.3	16.35
PFRC-0-2	21.33	1.30	0	42.96	22.87	PFRC-5-2	19.75	1.36	4.53	40.75	17.45
PFRC-0-3	24.15	1.56	0	46.03	24.90	PFRC-5-3	21.54	1.43	3.99	43.25	18.01
BFRC-0-1	22.50	1.31	0	42.58	24.53	BFRC-5-1	22.05	1.53	4.24	45.21	19.58
BFRC-0-2	21.90	1.57	0	42.55	23.46	BFRC-5-2	19.42	1.45	5.13	42.89	17.32
BFRC-0-3	25.50	1.60	0	45.37	27.29	BFRC-5-3	21.83	1.61	3.76	43.90	20.10
BPFRC-0-1	26.05	1.23	0	49.22	30.16	BPFRC-5-1	22.58	1.79	4.37	48.30	22.69
BPFRC-0-2	24.30	1.33	0	47.21	28.83	BPFRC-5-2	22.65	1.49	4.25	46.77	23.12
BPFRC-0-3	26.15	1.58	0	47.57	31.17	BPFRC-5-3	21.34	1.46	4.69	47.43	21.41
NC-2-1	20.42	1.55	1.80	42.23	20.65	NC-10-1	15.08	1.35	7.35	37.84	11.96
NC-2-2	20.01	1.36	1.45	43.27	19.60	NC-10-2	15.92	1.28	7.15	39.69	10.95
NC-2-3	19.18	1.60	1.91	42.00	18.18	NC-10-3	18.53	1.75	5.93	41.57	15.48
PFRC-2-1	22.67	1.66	1.47	45.77	20.62	PFRC-10-1	20.28	1.7	5.99	43.21	15.12
PFRC-2-2	23.14	1.72	1.59	46.4	21.19	PFRC-10-2	18.71	1.45	6.84	40.87	13.69
PFRC-2-3	22.32	1.50	1.87	47.33	20.14	PFRC-10-3	19.69	1.53	6.62	41.92	15.45
BFRC-2-1	22.64	1.39	1.50	47.58	22.03	BFRC-10-1	19.59	1.52	6.54	40.25	13.58
BFRC-2-2	21.93	1.56	1.96	46.60	20.00	BFRC-10-2	17.96	1.31	7.10	39.67	11.65
BFRC-2-3	23.74	1.68	1.38	46.82	24.92	BFRC-10-3	20.77	1.67	5.96	41.58	15.29
BPFRC-2-1	26.01	1.47	1.55	51.45	30.05	BPFRC-10-1	21.10	1.64	6.68	46.02	17.07
BPFRC-2-2	25.21	1.35	1.45	50.67	28.11	BPFRC-10-2	22.00	1.42	5.61	46.78	18.52
BPFRC-2-3	23.42	1.28	1.81	47.88	24.77	BPFRC-10-3	20.08	1.38	6.95	44.60	15.53

注:试件分组编号NC- $\eta_0$ -1中,NC表示普通混凝土, $\eta_0$ 表示理论锈蚀率,1表示第1个试件; $\tau_u$ 为黏结强度; $s_u$ 为峰值滑移; $K_i$ 为初始黏结刚度; $K_s$ 为割线黏结刚度。

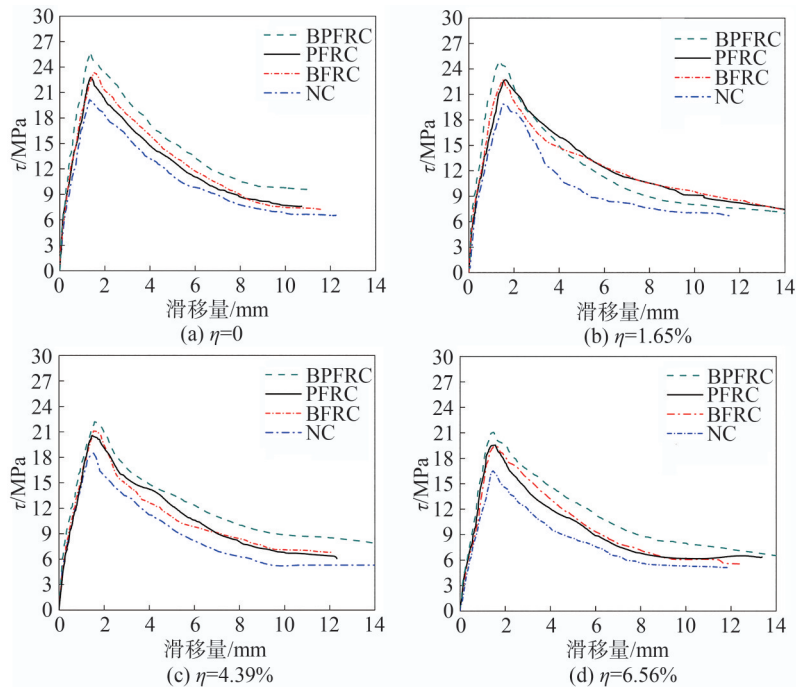


图 10 黏结-滑移曲线  
Fig. 10 Bond-slip curves

与钢筋之间的摩擦力和机械咬合力增大,曲线进入下降阶段,同时锈蚀引起的混凝土开裂会导致混凝土与钢筋间互锁作用显著减弱。当钢筋肋前的混凝土被压碎,滑移迅速增大,标志曲线进入残余阶段。随滑移量增加,黏结应力缓慢下降并趋于稳定。

从同一锈蚀率下不同FRC与NC的曲线走势可以发现后,纤维的掺入使钢筋与混凝土之间的黏结强度、黏结刚度和残余黏结应力均有所增加,下降段曲线更加平缓。

不同锈蚀率下,BPFRC整体表现最佳,其次为BFRC。体积掺量0.1%条件下BF对混凝土抗侵蚀的增强作用大于PF<sup>[16]</sup>。BF对氯盐有较高抗性,提高了混凝土的密实性从而保护内部钢筋免受锈蚀;此外BF属于亲水性纤维,可以与混凝土基体更好地牢固黏结,并在氯离子侵蚀时消耗部分膨胀应力。而PF是一种合成纤维,优势在于可提高混凝土的韧性和裂缝控制,但在抗侵蚀方面能力有限,与基体的黏结力相对较弱。

### 2.3.1 黏结强度

将最大黏结应力视为黏结强度,图11为锈蚀对黏结强度的影响。从图11可看出,随着钢筋锈蚀率的增加,黏结强度均表现出下降趋势。

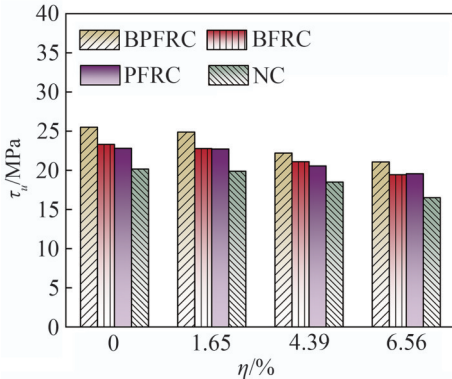


图 11 锈蚀对黏结强度影响

Fig. 11 Effects of corrosion on bond strength

在锈蚀率为0~2%范围内,没有观察到微锈蚀条件下黏结强度明显提高的现象<sup>[21]</sup>,可能由于产生不均匀锈蚀及锈胀裂缝的存在削弱了增强效果。平均锈蚀率在1.65%时,BPFRC、BFRC、PFRC和NC黏结强度相对于 $\eta=0$ 时分别降低了2.4%、2.3%、0.3%、1.4%。黏结强度在 $\eta$ 为2%~7%区间内快速下降,当锈蚀率接近5%时BPFRC黏结强度已降至未锈蚀试件的87%。当锈蚀率在6%~7%间,普通混凝土相比未锈蚀前黏结强度平均降低18.1%。随着锈蚀率增大,混凝土锈胀裂缝逐渐变宽,对钢筋的环向压应力减弱,降低了钢筋与混凝土间机械咬合作用。在不同锈蚀率下,纤维掺入对混凝土内部结构的改善减小了裂缝间隙;同时

增加混凝土与钢筋之间的界面摩擦力,提高了黏结面的粗糙度。不同锈蚀率下FRC黏结强度相比普通混凝土提高了11.1%~27.6%,其中,BPFRC比普通混凝土提高19.9%~27.6%,比单掺PF/BF时提高5.2%~11.8%,在黏结性能方面体现出正协同效应。

### 2.3.2 黏结刚度

黏结刚度是评价试件抵抗拉拔破坏能力的重要标准之一。从黏结滑移曲线中确定两个不同的黏结刚度值,分别为初始黏结刚度 $K_i$ (初始点处的刚度,本文取 $s=0.01$ )与割线黏结刚度 $K_h$ (峰值黏结应力一半时的刚度)。由式(5)计算刚度值:

$$K(s) = \frac{\tau(s)}{s} \quad (5)$$

式中, $K$ 为黏结刚度, $s$ 为对应滑移量。

从表4中还可以看出,FRC通常具有较高的初始黏结刚度和割线黏结刚度,纤维在提高混凝土约束方面发挥着积极作用,可有效延缓试件破坏,在一定程度上发挥支撑作用。黏结刚度与锈蚀程度间关系如图12所示,BPFRC、PFRC与BFRC初始黏结刚度在平均锈蚀率1.65%时相对于 $\eta=0$ 时,分别提高4.20%、5.20%、8.00%,锈蚀产物堆积增大了钢筋混凝土间摩擦,握裹力增强,故黏结刚度出现上升趋势。随锈蚀程度加深,保护层开裂导致混凝土的约束和界面摩擦大幅降低,以致割线黏结刚度产生明显下降,BPFRC与NC的割线刚度在锈蚀率达6.56%时相比未锈蚀时分别下降了43.30%和39.00%,而初始黏结刚度受锈蚀影响较小,仅降低了5.00%和11.80%。试验结果显示BF与PF对黏结刚度的改善效果并无明显差异,没有体现出BF高刚度、高强度特性,这与纤维掺量偏小导致了较大的分布离散性有关。而在BPFRC中表现出的刚度优势,归因于二者协同工作对裂缝控制的积极作用。

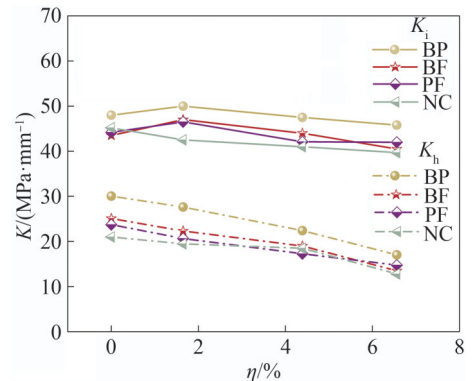


图 12 锈蚀对黏结刚度影响

Fig. 12 Effects of corrosion on bond stiffness

观察割线黏结刚度与黏结强度的变化趋势可以发现,二者较为相似,黏结强度越高,割线黏结刚度通常也越高,且均随锈蚀率的增加逐渐降低,这表明

二者之间可能存在相关性,黏结强度与割线黏结刚度、黏结强度与峰值滑移比值与割线黏结刚度的关系曲线分别见图 13 和 14,并利用 MATLAB 对关系曲线进行拟合,得到式(6)和(7):

$$K_h = 0.04\tau_u^2 + 0.998 \quad (6)$$

$$K_h = 2.168 \frac{\tau_u}{s_u} - 11 \quad (7)$$

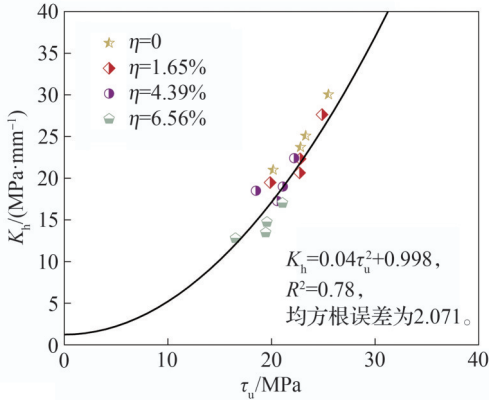


图 13 黏结强度与割线黏结刚度的关系

Fig. 13 Relationship between bond strength and secant bond stiffness

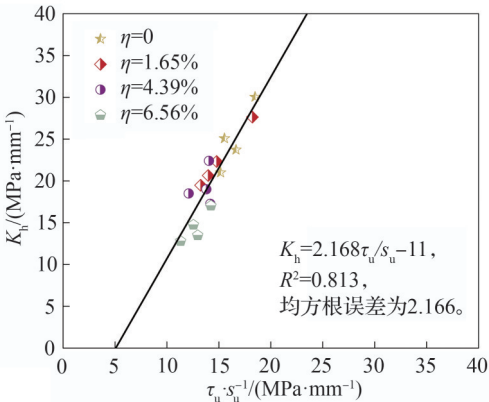


图 14 黏结强度与峰值滑移比值与割线黏结刚度的关系

Fig. 14 Relationship between the ratio of bond strength to peak slip and secant bond stiffness

受钢筋锈蚀的影响,刚度与强度设为二次函数关系进行拟合的结果较为理想,割线黏结刚度在锈蚀后退化更为严重。

### 2.3.3 峰值滑移

峰值滑移是钢筋和混凝土之间黏结性能的一个重要指标,随着钢筋锈蚀率的增加,钢筋表面积累的锈层会削弱钢筋与混凝土之间的初始黏结力,同时锈胀裂缝的产生使混凝土结构完整性受损,在加载时钢筋更容易滑动。由表 4 测试结果看出,NC 在各理论锈蚀率下的平均峰值滑移为 1.33、1.50、1.53 和 1.46 mm。在相同锈蚀条件下,FRC 较 NC 峰值滑移并无规律性变化,总体上呈先增加后下降趋势,在一定程度上受到混凝土开裂影响但变化并不明显。

## 2.4 SEM 测试分析

纤维与混凝土基体的良好黏结是发挥作用的前提,对钢筋混凝土的黏结段取样进行电镜扫描,玄武岩与聚丙烯纤维-水泥界面过渡区的微观结构如图 15 所示。从图 15 可以看出,拉拔试验后 BF 被折断、脱落、无明显弯曲变形,说明 BF 具有较高的弹性模量,发挥了桥接作用并吸收部分能量;PF 出现了拔出伸长现象,其对宏观裂缝扩展具有更明显的抑制作用。在混凝土内部,掺入纤维一定程度上细化了孔隙结构,减少了砂浆-骨料界面过渡区、孔隙间的微裂缝,弱化了初始缺陷,从而提高对损伤的耐受程度,纤维作用机理如图 16 所示。纤维的阻裂作用归因于水泥浆对纤维的牢固抓持,纤维将自身的拉力传递给周围混凝土,延长了应力传递路径,从而消耗了更多的能量,从图 16 可见纤维提高了基体的力学性能。但过多相互重叠搭接的纤维不仅起不到阻裂作用<sup>[22]</sup>,反而会因水泥浆体不能完全填充纤维间的空隙,导致无法形成有效的包裹加速裂缝扩展。通过 SEM 观察纤维并未产生明显集聚,纤维随机分布建立的 3 维网络结构增强了骨料和水泥浆体之间的结合,从而增强了混凝土的整体完整性。

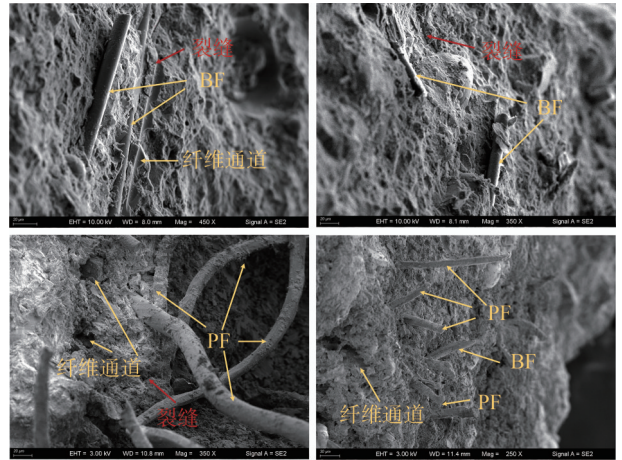


图 15 玄武岩与聚丙烯纤维-水泥界面过渡区

Fig. 15 Basalt fiber and polypropylene fiber-cement interfacial transition zone

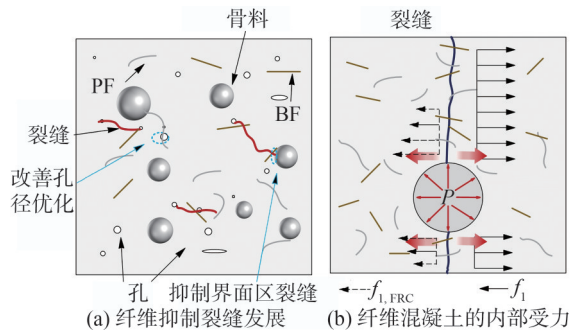


图 16 纤维作用机理

Fig. 16 Fiber action mechanism

由图 16 可知,当钢筋与混凝土间发生剪切破坏时,径向应力  $P$  随荷载的增加而增大,引起的开裂力  $f_f$  由 FRC 抗拉强度抵抗,正是由于纤维桥接效应及箍筋提供了足够的约束,试件并未发生劈裂破坏,使 FRC 在黏结性能上较 NC 表现出一定优势。

### 3 黏结-滑移本构模型

#### 3.1 黏结强度计算

以往对 FRC 研究很少考虑黏结锈蚀损伤。故引入锈蚀损伤系数  $\lambda_c$  来考虑滨海环境氯离子侵入造成的影响。

$$\tau_u = \lambda_c \tau_0 \quad (8)$$

式中,  $\tau_0$  为未锈蚀时的黏结强度。

FRC 的  $\tau_0$  取决于多种因素,包括纤维长径比、纤维掺量等。为量化裂纹处纤维对环向应力的贡献,本文基于纤维基体离散模型<sup>[23]</sup>计算 FRC 的  $\tau_0$ , 见式(9)、(10),普通混凝土  $\tau_0$  的计算采用 FIB—2010 规范<sup>[24]</sup>建议的经验方程。

$$\tau_0 = \frac{1.28\phi c \tau_b \rho_f l_f}{\pi d_r d} \quad (9)$$

$$\phi = \frac{\sin \beta + \mu \cos \beta}{\cos \beta - \mu \sin \beta} \quad (10)$$

式(9)~(10)中:  $\beta$  为有效分离角 ( $30^\circ \sim 40^\circ$ );  $\mu$  为摩擦系数;  $c$  为保护层厚度;  $\rho_f$  为纤维掺量;  $\tau_b$  为纤维与基体的黏结强度,光滑纤维取 10 MPa。

从图 11 中还可以看出,随着锈蚀程度的变化,黏结强度并没有如一次函数般下降,轻微锈蚀阶段下降并不明显。故为了更好地体现变化规律,本文  $\lambda_c$  采用 2 次线性多项式(式(11))来拟合数据:

$$\lambda_c = a\eta^2 + b\eta + c \quad (11)$$

式中,  $a, b, c$  为拟合系数。

将确定参数代入式(9)和(11)与规范[24],得到不同 FRC 黏结强度计算方程:

$$\tau_u = \begin{cases} (-0.0026\eta^2 - 0.032\eta + 1.72)\tau_{0PB}, R^2 = 0.895; \\ (-0.0043\eta^2 - 0.01\eta + 1.48)\tau_{0PF}, R^2 = 0.926; \\ (-0.0049\eta^2 - 0.015\eta + 1.64)\tau_{0BF}, R^2 = 0.884; \\ (-0.0046\eta^2 + 0.0027\eta + 0.97)\tau_0, R^2 = 0.932 \end{cases} \quad (12)$$

由于缺乏对混掺纤维协同作用在黏结性能方面更深入的研究,本文没有进行不同掺量的对比,混掺纤维的贡献在方程中只是数值上的叠加。

图 17 为考虑锈蚀影响下的黏结强度计算值与试验值比较,已有研究尚少,故对钢-聚丙烯纤维混凝土<sup>[25]</sup>进行验证,发现虽然钢纤维与玄武岩纤维在混凝土增强增韧性方面有相似优势,但纤维自身特征

参数及抵抗侵蚀能力上的差异使结果离散性较大,此外验证结果良好。考虑到试验设置横向约束使计算值结果偏大,可在纤维参数、配箍率方面进一步优化。

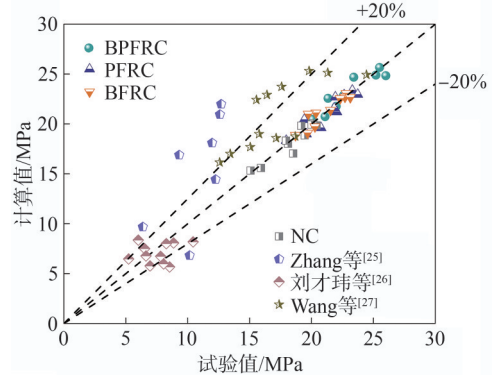


图 17 锈蚀试件黏结强度计算值与试验值的对比

Fig. 17 Comparison between the calculated and experimental bond strength values of corroded specimens

#### 3.2 残余黏结强度

残余黏结强度是评价钢筋混凝土结构残余承载能力的重要依据,它可以被视为黏结滑移本构模型中下降阶段和残余阶段的控制点,可通过与钢筋肋间距(本文中为 10 mm)相等的滑移值所对应的黏结应力计算:

$$\tau_r = \zeta \tau_u \quad (13)$$

式中,  $\zeta$  为残余黏结强度控制系数,  $\tau_r$  为残余黏结强度。

残余黏结强度系数试验数据如图 18 所示。从图 18 可以看出,不同锈蚀程度下的  $\zeta$  值较均匀分布在平均值 0.351 上下。这表明残余黏结强度基本不受锈蚀因素的影响,但 FRC 的残余黏结强度 (BPFRC: 0.371, BFRC: 0.362, PFRC: 0.347) 较 NC (0.324) 有所提高,在破坏过程中,纤维的抵抗拉伸及抑制裂缝发展能力发挥重要作用。

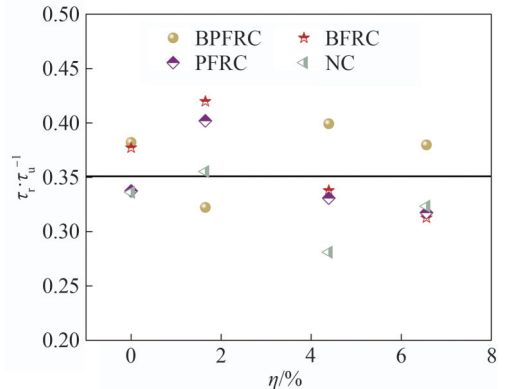


图 18 残余黏结强度系数

Fig. 18 Residual bond strength factors

#### 3.3 黏结滑移本构模型

通过研究黏结关系,有些学者提出相关的本构模型,归纳如表 5 所示。从表 5 可以看出,采用分段方程的

形式进行描述更为准确,可引入不同参数来考虑材料和锈蚀的影响,因此本文采用三段式建立 FRC 与锈蚀钢筋之间的黏结滑移本构模型,表 5 中,  $s_r$  为残余滑移。

使用 MATLAB 软件对实验数据进行回归分析,得

到不同工况条件下黏结滑移曲线上升段的参数  $\alpha$ ,拟合结果见表 6。FRC 与 NC 对应的参数  $\alpha$  随锈蚀率的增加而增加,这与氯离子侵蚀后曲线上升阶段斜率即刚度减小有关。

表 5 黏结滑移本构模型总结

Tab. 5 Summary of the bond-slip ontological model

文献来源	本构模型	参数值	适用范围
Lee 等 <sup>[28]</sup>	$\tau = \begin{cases} \left(\frac{s}{s_u}\right)^\alpha, & s \leq s_1; \\ \tau_u, & s_1 < s \leq s_2; \\ \frac{s_3-s}{s_3-s_2}(\tau_u - \tau_r) + \tau_r, & s_2 < s \leq s_3; \\ \tau_r, & s_3 \leq s \end{cases}$	$\alpha=0.5$	NC 未锈蚀
Shi 等 <sup>[29]</sup>	$\frac{\tau}{\tau_u} = \begin{cases} \alpha_1 \frac{s}{s_u} + \frac{n-(n-1)\alpha_1}{n-t} \left(\frac{s}{s_u}\right)^t + \frac{-t+(t-1)\alpha_1}{n-t} \left(\frac{s}{s_u}\right)^n, & 0 \leq \frac{s}{s_u} < 1; \\ \frac{s}{b\left(\frac{s}{s_u}-1\right)^\lambda s_u + s}, & \frac{s}{s_u} \geq 1, b \geq 0, \lambda \geq 1 \end{cases}$	$\alpha_1, n, t, b, \lambda$ 根据文献[29]计算	SMA-FRC 未锈蚀
Zhang 等 <sup>[30]</sup>	$\tau = \begin{cases} \left(\frac{s}{s_u}\right)^\alpha \tau_u, & 0 \leq s < s_u; \\ \left(1.0 - 0.7 \times \frac{s-s_u}{s_r-s_u}\right) \tau_u, & s_u \leq s < s_r; \\ \tau_r = \varphi \tau_u, & s \geq s_r \end{cases}$	$\alpha=0.4,$ $\varphi=0.3$	NC 钢筋锈蚀/高温
Chen <sup>[11]</sup>	$\tau = \begin{cases} \tau_u \left(2 \sqrt{\frac{s}{s_u}} - \frac{s}{s_u}\right), & 0 \leq s < s_u; \\ \tau_u \frac{(s_r-s)^2 (s_r-0.243s-0.757s_u)}{(s_r-s_u)^3} + \tau_r \frac{(s-s_u)^2 (1.61s_r-0.61s-s_u)}{(s_r-s_u)^3}, & s_u \leq s < s_r; \\ \tau_r, & s \geq s_r \end{cases}$	$\tau_u, \tau_r, s_u$ 根据文献[11]计算	FRC 未锈蚀
本文	$\tau = \begin{cases} \left(\frac{s}{s_u}\right)^\alpha \tau_u, & 0 \leq s < s_u; \\ \frac{\tau_r - \tau_u}{s_r - s_u} (s - s_u) + \tau_u, & s_u \leq s < s_r; \\ \zeta \tau_u, & s \geq s_r \end{cases}$	$\alpha$ 的取值根据表 6 计算, $\zeta=0.351$	FRC 锈蚀

表 6 拟合结果

Tab.6 Fitting results

纤维类型	$\eta_0/\%$	$\alpha$	$R^2$	纤维类型	$\eta_0/\%$	$\alpha$	$R^2$
BP	0	0.47	0.957	BP	5	0.48	0.969
PF	0	0.51	0.939	PF	5	0.58	0.905
BF	0	0.52	0.950	BF	5	0.52	0.941
NC	0	0.51	0.941	NC	5	0.53	0.976
BP	2	0.48	0.964	BP	10	0.55	0.949
PF	2	0.53	0.959	PF	10	0.59	0.922
BF	2	0.56	0.962	BF	10	0.60	0.870
NC	2	0.54	0.951	NC	10	0.61	0.881

为验证黏结滑移本构模型的准确性,将部分试验数据与计算结果进行比较,如图 19 所示。从图 19 可以看出,曲线下降段试验值偏低,但整体走势基本能保证误差在 20% 以内。该模型可为 BF-PF 增强混凝土性能评估提供参考,对于其他类型或不同体积掺量的 FRC 的适用性有待验证。

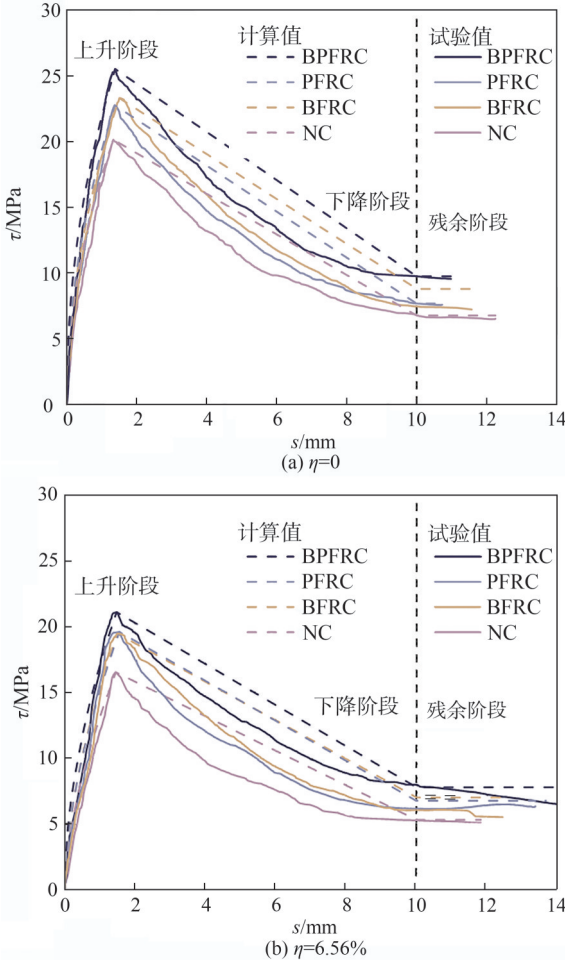


图 19 部分计算值与试验值的比较

Fig. 19 Comparison of some calculated and tested values

## 5 结论

本文对锈蚀钢筋与 BF-PF 增强混凝土间的黏结性能进行了试验研究,探究了不同损伤条件下纤维掺入对黏结退化的影响,横向对比不同 FRC 与 NC 间差异,基于研究结果可以得出以下结论:

1) 掺入体积分数 0.1% 的 BF、PF 提高了混凝土的力学性能,其中 BF 对抗压强度和抗折强度的影响优于 PF,当两种纤维混合时,其在混凝土开裂变形过程中发挥着互补作用,体现出的正协同效应对劈裂抗拉强度改善最为明显。

2) FRC 在黏结性能上有更好的表现,不同锈蚀率下 FRC 的黏结强度比普通混凝土提高 11.1%~27.6%,

割线黏结刚度与黏结强度、黏结强度与峰值滑移成正比相关。

3) 钢筋锈蚀后,由于锈蚀产物堆积膨胀产生环向拉应力,使混凝土保护层开裂黏结强度下降。在有横向约束条件下 FRC 比普通混凝土的下降趋势更加平缓且残余强度更高,纤维掺入有效延缓了试件的破坏,能够吸收部分能量并在一定程度上发挥支撑作用。

4) 在黏结强度预测公式和三段式本构模型中试验值与计算结果吻合较好,但存在一定的局限性:混掺的影响仅为数值的叠加,侧重点在横向对比不同纤维影响下差异,缺乏同种纤维掺量或长径比的变化,后续可在此方面进一步修正。

参考文献:

- [1] Zheng Yuanxun, Fan Congcong, Ma Junjie, et al. Review of research on Bond-Slip of reinforced concrete structures[J]. Construction and Building Materials, 2023, 385: 131437.
- [2] Qu Fulin, Li Wengui, Dong Wenkui, et al. Durability deterioration of concrete under marine environment from material to structure: A critical review[J]. Journal of Building Engineering, 2021, 35: 102074.
- [3] Yalciner H, Eren O, Sensoy S. An experimental study on the bond strength between reinforcement bars and concrete as a function of concrete cover, strength and corrosion level[J]. Cement and Concrete Research, 2012, 42(5): 643-655.
- [4] Wang Zhaoyang, Yang Ou, Huo Jingsi. Experimental study on bond performance between corroded reinforced bar and concrete[J]. Journal of Harbin Institute of Technology, 2018, 50(8): 150-155. [王朝阳, 杨鸥, 霍静思. 锈蚀钢筋与混凝土间黏结性能试验[J]. 哈尔滨工业大学学报, 2018, 50(8): 150-155.]
- [5] Li Qiang, Tian Ye, Fang Deming, et al. The influence of longitudinal rebar type and stirrup ratio on the bond performance of reinforced concrete with corrosion[J]. Construction and Building Materials, 2023, 409: 133943.
- [6] Yang Lu, Zheng Shansuo, Zheng Yue, et al. Bond-slip constitutive model of corroded reinforced concrete and its numerical simulation application[J]. Journal of Harbin Institute of Technology, 2024, 56(1): 139-150. [杨路, 郑山锁, 郑跃, 等. 锈蚀钢筋混凝土黏结滑移本构模型及数值模拟应用[J]. 哈尔滨工业大学学报, 2024, 56(1): 139-150.]
- [7] Zhao Chenggong, Wang Zhiyuan, Zhu Zhenyu, et al. Research on different types of fiber reinforced concrete in recent years: An overview[J]. Construction and Building Materials, 2023, 365: 130075.

- [8] Shi Feng, Pham T M, Hao Hong, et al. Post-cracking behaviour of basalt and macro polypropylene hybrid fibre reinforced concrete with different compressive strengths[J]. *Construction and Building Materials*, 2020, 262: 120108.
- [9] Hou Lijun, Sun Hui, Liu Gengsheng, et al. Bond strength of deformed reinforcement embedded in steel fiber reinforced concrete: Influencing factors and prediction model [J]. *Construction and Building Materials*, 2023, 407: 133436.
- [10] Zhang He, Li Huiyan, Lin Tengxin, et al. Experimental investigation on influence of embedment length, bar diameter and concrete cover on bond between reinforced bars and steel fiber reinforced concrete (SFRC) [J]. *Case Studies in Construction Materials*, 2024, 21: e03742.
- [11] Chen Yuxiu, Zhao Yunfeng, Zeng Lei, et al. Bond performance and bond-slip constitutive model for rebar embedded in rubber powder-modified polypropylene fiber reinforced concrete[J]. *Construction and Building Materials*, 2023, 375: 130934.
- [12] Shatarat N, Katkhuda H, Ayyoub M, et al. Improving bond strength of recycled coarse aggregate concrete using chopped basalt fibers[J]. *Case Studies in Construction Materials*, 2022, 17: e01449.
- [13] de Melo F M C, de Jesus Cruz A C A, de Souza Netto L D, et al. Experimental study of bond between steel bars and hybrid fibers reinforced concrete[J]. *Construction and Building Materials*, 2021, 275: 122176.
- [14] Xu Lihua, Zhang Aoli, Huang Le, et al. Study on bond strength between steel-polypropylene hybrid fiber reinforced concrete and deformed bar under cyclic loading[J]. *Journal of Building Structures*, 2017, 38(11): 149–158. [徐礼华, 张奥利, 黄乐, 等. 反复荷载作用下钢-聚丙烯混杂纤维混凝土与钢筋黏结强度研究[J]. *建筑结构学报*, 2017, 38(11): 149–158.]
- [15] Hu Xinyu, Guo Yihong, Lv Jianfu, et al. The mechanical properties and chloride resistance of concrete reinforced with hybrid polypropylene and basalt fibres[J]. *Materials*, 2019, 12(15): 2371.
- [16] Li Zhongxian, Li Changhui, Shi Yundong, et al. Experimental investigation on mechanical properties of hybrid fibre reinforced concrete[J]. *Construction and Building Materials*, 2017, 157: 930–942.
- [17] 中华人民共和国住房和城乡建设部. 混凝土物理力学性能试验方法标准[GB/T 50081—2019][S]. 北京: 中国建筑工业出版社, 2019.
- [18] Smarzewski P. Influence of basalt-polypropylene fibres on fracture properties of high performance concrete[J]. *Composite Structures*, 2019, 209: 23–33.
- [19] Zhao Bingbing, He Jingjing, Wang Xuezhi, et al. Experimental study on mechanical properties of basalt-polypropylene hybrid fiber reinforced concrete[J]. *China Concrete and Cement Products*, 2014(8): 51–55. [赵兵兵, 贺晶晶, 王学志, 等. 玄武岩-聚丙烯混杂纤维混凝土基本力学性能试验研究[J]. *混凝土与水泥制品*, 2014(8): 51–55.]
- [20] Wang Chengqi, Wu Keru. Research on the hybrid effect of different geometrical size hybrid fiber reinforced concrete [J]. *Journal of Building Materials*, 2005, 8(3): 250–255. [王成启, 吴科如. 不同几何尺寸纤维混杂混凝土的混杂效应[J]. *建筑材料学报*, 2005, 8(3): 250–255.]
- [21] Fu Chuanqing, Fang Deming, Ye Hailong, et al. Bond degradation of non-uniformly corroded steel rebars in concrete [J]. *Engineering Structures*, 2021, 226: 111392.
- [22] Huo Linying, Bi Jihong, Zhao Yun, et al. Constitutive model of steel fiber reinforced concrete by coupling the fiber inclining and spacing effect[J]. *Construction and Building Materials*, 2021, 280: 122423.
- [23] Qi Jianan, Cheng Zhao, Ma Z J, et al. Bond strength of reinforcing bars in ultra-high performance concrete: Experimental study and fiber-matrix discrete model[J]. *Engineering Structures*, 2021, 248: 113290.
- [24] fib-federation internationale du beton. fib model code for concrete structures 2010[M]. Switzerland: John Wiley & Sons, 2013.
- [25] Zhang Qiang, Lu Zhaohui, Li Jintong, et al. Impact of cyclic loading and corrosion on the bond performance of steel-polypropylene hybrid fiber reinforced concrete[J]. *Materials and Structures*, 2024, 57(3): 46.
- [26] Liu Caiwei, Yan Liangtai, Ba Guangzhong, et al. Experimental investigation on bond performance of corroded reinforced concrete after exposure to high temperature[J]. *Journal of Building Structures*, 2023, 44(3): 257–267. [刘才玮, 闫良泰, 巴光忠, 等. 锈蚀钢筋与混凝土高温后黏结性能试验研究[J]. *建筑结构学报*, 2023, 44(3): 257–267.]
- [27] Wang Dehong, Han Lei, Kang Mengxin, et al. Influence of corrosion on the bond performance of reinforcements and basalt fibre high strength concrete[J]. *Case Studies in Construction Materials*, 2022, 17: e01394.
- [28] Lee S W, Kang Shaobo, Tan Kanghai, et al. Experimental and analytical investigation on bond-slip behaviour of deformed bars embedded in engineered cementitious composites[J]. *Construction and Building Materials*, 2016, 127: 494–503.
- [29] Shi Mingfang, Xu Guangping, Zhao Jitao, et al. The study on bond-slip constitutive model of shape memory alloy

fiber-reinforced concrete[J]. *Construction and Building Materials*, 2024, 418: 135395.

performance of corroded steel bars in concrete after high temperature exposure[J]. *Engineering Structures*, 2019, 198: 109479.

[30] Zhang Bai, Zhu Hong, Chen Jun, et al. Evaluation of bond

## Experimental Study on the Bond Performance Between Corroded Steel Bar and Fiber-reinforced Concrete

LIU Yanchun<sup>1</sup>, CHEN Bensheng<sup>1</sup>, LIU Caiwei<sup>1\*</sup>, YAN Liangtai<sup>2</sup>, LIU Xinyu<sup>1</sup>, MIAO Jijun<sup>1</sup>

(1. School of Civil Engineering, Qingdao University of Technology, Qingdao 266520, China;

2. College of Architecture and Civil Engineering, Beijing University of Technology, Beijing 100124, China)

### Abstract:

**Objective** Reinforced concrete structures remain highly vulnerable to chloride ion corrosion during prolonged service life. Fiber-reinforced concrete (FRC) demonstrates enhanced durability, making it well-suited for complex environments and rigorous engineering demands. This study seeks to clarify the influence of fiber incorporation on the concrete matrix and to examine the variation in bond performance between different types of FRC and corroded steel reinforcement.

**Methods** A total of 36 specimens were designed for basic mechanical performance testing, and eccentric pull-out tests were conducted on 48 prism specimens subjected to varying corrosion rates (0, 2%, 5%, and 10%). The corrosion of the steel reinforcement was accelerated using electrochemical methods. Stirrups were incorporated into the specimens without insulation or oxygen isolation treatment to simulate actual engineering conditions. A corrosion current density of 200  $\mu\text{A}/\text{cm}^2$  was maintained. The relationship between the applied time and the theoretical corrosion rate was determined based on Faraday's law. After reaching the predetermined corrosion time, the specimens were dried and then subjected to pull-out tests. The pull-out force was measured using sensors on the testing machine, while two Linear Variable Differential Transformers (LVDTs) recorded slip values. Tests were performed using a displacement-controlled loading method at a rate of 0.5 mm/min, and the pull-out process was terminated when the pull-out force stabilized or the specimen failed. Surface changes and failure modes were documented. The bonded steel was extracted, rust was removed through acid washing, and the actual corrosion rate of the steel reinforcement was calculated using the mass loss method. Scanning electron microscopy (SEM) was then employed for microscopic analysis of the bonded interface after failure. SEM observations revealed the microstructure of the basalt-polypropylene fiber-cement interfacial transition zone, as well as the distribution and post-failure morphology of the fibers, which further clarified the fiber action mechanisms. Based on the experimental results and incorporating the corrosion damage factor, semi-empirical and semi-theoretical bond strength prediction formulas, together with a three-segment bond-slip constitutive model, were developed for different fiber incorporations. These models generally maintained errors within 20%, which confirmed their effectiveness and accuracy.

**Results and Discussions** In terms of mechanical properties, fiber bridging effectively inhibited crack development and dispersed the applied loads. The incorporation of basalt fibers (BF) and polypropylene fibers (PF) into the concrete resulted in a more pronounced improvement in splitting tensile strength, with splitting tensile strength and flexural strength increasing by 12.43%~18.65% and 5.36%~9.64%, respectively. BF restricted the initiation and propagation of microcracks, while PF primarily limited the expansion of macrocracks after their formation, demonstrating a positive synergistic effect of PF+BF. An analysis of the specimens' appearance after corrosion indicated that corrosion products accumulated between the steel reinforcement and the concrete. As corrosion advanced, rust-induced swelling cracks formed on the concrete surface, accompanied by the overflow of reddish-brown rust products. The incorporation of fibers modified the concrete's porosity and permeability, and factors such as corrosion discretization caused actual corrosion rates to be lower than theoretical values. Due to the bridging effect of fibers and the lateral confinement provided by stirrups, all specimens failed in splitting pull-out. FRC specimens exhibited finer and fewer cracks than normal concrete (NC) specimens. Primary cracks extended toward the concrete side and, as the load increased, developed into longitudinal through-cracks parallel to the steel reinforcement, ultimately leading to the ductile failure of the specimens. Bond strength degraded significantly with increasing corrosion rates in terms of bond performance. When the corrosion rate reached approximately 5%, the bond strength of BPFRC decreased to 87% of that of the non-corroded specimens. When steel mass loss ranged between 6% and 7%, the bond strength of NC decreased by an average of 18.1%. Under corrosive conditions, the bond strength of FRC increased by 11.1%~27.6% compared to NC, with BPFRC exhibiting improvements of 19.9%~27.6%, which was 5.2%~11.8% higher than that of specimens with single PF or BF additions, indicating a positive synergistic effect. In addition, FRC demonstrated higher initial and secant bond stiffness. At an average corrosion rate of 1.65%, the accumulation of corrosion products increased the friction between the steel reinforcement and the concrete, which resulted in an increase in the initial bond stiffness of BPFRC, PFRC, and BFRC by 4.2%, 5.2%, and 8.0%, respectively. However, as corrosion progressed, cracking of the protective layer sig-

nificantly reduced concrete confinement and interface friction. At a corrosion rate of 6.56%, the secant bond stiffness of BPFRC and NC decreased by 43.3% and 39.0%, respectively, while the initial bond stiffness was less affected, decreasing by 5.0%~11.8%. Under the same lateral confinement conditions, FRC exhibited a more gradual decline and higher residual bond strength compared to NC. Fiber incorporation effectively delayed specimen failure, absorbed part of the energy, and provided additional structural support. No consistent patterns were identified in the changes of slip amounts among different FRCs and NC under identical corrosion conditions, where an initial increase was followed by a decrease. This behavior was partly influenced by concrete cracking but remained relatively stable.

**Conclusions** The experimental results confirm that corrosion damage is a critical factor influencing the bond performance between steel reinforcement and concrete. As the corrosion rate increases, bond degradation becomes more severe. Fiber-reinforced concrete, compared to normal concrete, demonstrates improvements in both fundamental mechanical properties and bond performance after corrosion damage. Appropriate fiber additions mitigate initial defects in the concrete and effectively suppress crack propagation. A bond strength prediction formula and a constitutive relationship for fiber-reinforced concrete under corrosion influence were established. This research provides data support for evaluating the performance of BF-PF reinforced concrete and provides a theoretical basis for practical engineering applications.

**Key words:** fiber reinforced concrete; corrosion; mechanical properties; bond-slip; constitutive model

(编辑 张 琼)

引用格式: Liu Yanchun, Chen Bensheng, Liu Caiwei, et al. Experimental study on the bond performance between corroded steel bar and fiber-reinforced concrete[J]. *Advanced Engineering Sciences*, 2025, 57(5): 261-273. [刘延春, 陈本晟, 刘才玮, 等. 锈蚀钢筋与纤维增强混凝土黏结性能试验研究[J]. *工程科学与技术*, 2025, 57(5): 261-273.]